arXiv:1704.03917v1 [cond-mat.mtrl-sci] 12 Apr 2017

Spin Hall effect emerging from a chiral magnetic lattice without spin-orbit coupling

Yang Zhang,[1,2] Jakub Železný,[1] Yan Sun,[1] Jeroen van den Brink,[2] and Binghai Yan[3,*]

[1] *Max Planck Institute for Chemical Physics of Solids, 01187 Dresden, Germany*

[2] *Leibniz Institute for Solid State and Materials Research, IFW Dresden, 01069 Dresden, Germany*

[3] *Department of Condensed Matter Physics, Weizmann Institute of Science, 7610001 Rehovot, Israel*

Abstract

The spin Hall effect (SHE), which converts a charge current into a transverse spin current, has long been believed to be a phenomenon induced by the spin–orbit coupling. Here, we propose an alternative mechanism to realize the intrinsic SHE through a chiral magnetic structure that breaks the spin rotation symmetry. No spin–orbit coupling is needed even when the scalar spin chirality vanishes, different from the case of the topological Hall effect. In known chiral antiferromagnetic compounds Mn_3X (X = Ga, Ge, and Sn), for example, we indeed obtain large spin Hall conductivities based on *ab initio* calculations. Apart further developing the conceptual understanding of the SHE, our work suggests an alternative strategy to design spin Hall materials without involving heavy elements, which may be advantageous for technological applications.

Introduction – The spin Hall effect (SHE) [1] is one of the most important ways to create and detect spin currents in the field of spintronics, which aims to realize low-power-consumption and high-speed devices [2]. It converts electric currents into transverse spin currents and vice versa. The SHE in materials is generally believed to rely on spin–orbit coupling (SOC) [1, 3–5, for review]. In typical SHE devices, the generated spin current is injected into a ferromagnet (FM) and consequently switches its magnetization via the spin-transfer torque [6, 7] or drives an efficient motion of magnetic domain walls [8, 9].

The SHE is conceptually similar to the well established anomalous Hall effect (AHE). In recent decades, the understanding of the intrinsic AHE [10] and intrinsic SHE [11, 12] reached great success based on the concept of the Berry phase [13], which originates directly from the electronic band structure. Although the AHE requires the existence of SOC in a FM, it also appears in a non-coplanar magnetic lattice without SOC, where an electron acquires a Berry phase by hopping through sites with a chiral magnetic structure (nonzero scalar spin chirality) [14, 15], later referred as the topological Hall effect (THE) [16]. Thus, in experiment the THE-induced Hall signal is treated as a signature of the skyrmion phase with chiral spin texture (for instance Refs. 17 and 18). Provoked by the THE, recent numerical simulations of the spin scattering by a single skyrmion indicated a nonzero SHE without considering SOC [19, 20]. However, fundamental questions are still open. Is the skyrmion-like nonzero spin chirality always necessary? What is the generic condition for a SHE without SOC? Furthermore, heavy elements are found to enhance the Gilbert damping [7, 21] that hinders the spin-current-switching in an adjacent thin-film magnet, although the search for SHE compounds focuses on materials with strong SOC [22, 23]. From a technological point of view, SHE materials with negligible or weak SOC will bring an advantage to constrain the Gilbert damping.

The crucial role of SOC is to break the spin rotational symmetry (SRS) in SHE. Alternatively, noncollinear magnetic textures can also violate SRS. Therefore, we propose a mechanism to realize the SHE with the chiral magnetic structure but without SOC. Different from the THE in symmetry, such an SHE appears generally for the chiral magnetic lattice, even with zero scalar spin chirality. Here, we first prove the principle from the symmetry analysis in a simple lattice model. Then, we demonstrate the existence of a strong SHE in several known materials Mn_3X (X =Ga, Ge, and Sn)[24, 25] by *ab initio* calculations, both with and without SOC.

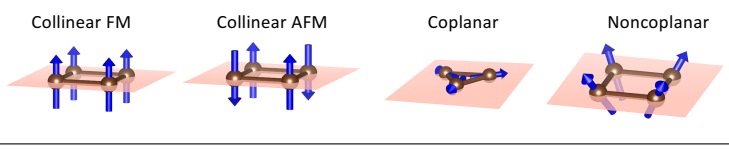

		Collinear FM	Collinear AFM	Coplanar	Noncoplanar
Without SOC	AHE	F	F	F	A
	SHE	F	F	A	A
With SOC	AHE	A	F	A	A
	SHE	A	A	A	A

FIG. 1. Existence of AHE and SHE in collinear FM, collinear AFM, coplanar, and noncoplanar chiral magnetic lattices with and without SOC. We can deduce whether AHE and SHE are allowed (A) or forbidden (F) by considering the symmetry. Regardless of SOC, the AHE is forbidden in a collinear AFM caused by the time-reversal symmetry combined with a half-lattice translation or an inversion. In addition, a nonmagnetic system that respects time-reversal symmetry is equivalent to a collinear AFM for both SHE and AHE.

Double-exchange model and symmetry analysis – We first consider a simple model to illustrate the symmetry of SHE without SOC. We employed a double-exchange model (s-d model) [26–28] which describes itinerant s electrons interacting with local d magnetic moments. Here we assume that magnetic moments are only contributed by the spin degrees of freedom.

$$H = t \sum_{<ij>\alpha} c^{\dagger}_{i\alpha} c_{j_\alpha} - J \sum_{i\alpha\beta} (\boldsymbol{\sigma} \cdot \boldsymbol{n}_i)_{\alpha\beta} c^{\dagger}_{i\alpha} c_{i\beta}. \tag{1}$$

Here, α and β stand for spin up and spin down, respectively. The first term is the nearest neighbor hopping term with $< ij >$ denoting the nearest neighbor lattice sites. In the second term, J is the Hund's coupling strength between the conduction electron and the on-site spin moment, $\boldsymbol{\sigma}$ is the vector of Pauli matrices, and $\boldsymbol{n}_i$ is the spin magnetic moment on site i. The magnetic texture is defined by the pattern of $\boldsymbol{n}_i$.

The intrinsic AHE and intrinsic SHE are well characterized via the Berry curvature formalism [1, 5, 10, 13]. The anomalous Hall conductivity(AHC) $\sigma_{\alpha\beta}$ can be evaluated by the integral of the Berry curvature $\Omega^n_{\alpha\beta}(\mathbf{k})$ over the Brillouin zone (BZ) for all the occupied bands, where n is the band index. This method can also be applied to the THE [14], even if it is commonly interpreted using the real space spin texture. Here, $\sigma_{\alpha\beta}$ corresponds to a 3×3 matrix and indicates a transverse Hall current j_α generated by a longitudinal electric field

E, which satisfies $J_\alpha = \sigma_{\alpha\beta}E_\beta$. Within a linear response, Berry curvature can be expressed as

$$\Omega_{n,\alpha\beta}(\vec{k}) = 2i\hbar^2 \sum_{m\neq n} \frac{\langle\psi_{n\mathbf{k}}|\,\hat{v}_\alpha\,|\psi_{m\mathbf{k}}\rangle\,\langle\psi_{m\mathbf{k}}|\,\hat{v}_\beta\,|\psi_{n\mathbf{k}}\rangle}{(E_n(\vec{k}) - E_m(\vec{k}))^2}, \tag{2}$$

where n and m are band indices, and $\psi_{n\mathbf{k}}$ and $E_{n\mathbf{k}}$ denote the Bloch wave functions and eigenvalues, respectively, and $\hat{\mathbf{v}}$ is the velocity operator. Replacing the velocity operator with the spin current operator $\hat{J}^\gamma_\alpha = \frac{1}{2}\{\hat{v}_\alpha, \hat{s}_\gamma\}$, where $\hat{s}_\gamma$ is the spin operator, we obtain the spin Berry curvature and corresponding spin Hall conductivity (SHC),

$$\begin{aligned} \sigma^\gamma_{\alpha\beta} &= \frac{e}{\hbar}\sum_n \int_{BZ} \frac{d^3\mathbf{k}}{(2\pi)^3} f_n(\mathbf{k})\Omega^\gamma_{n,\alpha\beta}(\mathbf{k}), \\ \Omega^\gamma_{n,\alpha\beta}(\mathbf{k}) &= 2i\hbar^2 \sum_{m\neq n} \frac{\langle\psi_{n\mathbf{k}}|\,\hat{J}^\gamma_\alpha\,|\psi_{m\mathbf{k}}\rangle\,\langle\psi_{m\mathbf{k}}|\,\hat{v}_\beta\,|\psi_{n\mathbf{k}}\rangle}{(E_{n\mathbf{k}} - E_{m\mathbf{k}})^2}. \end{aligned} \tag{3}$$

The SHC ($\sigma^\gamma_{\alpha\beta}$; $\alpha,\beta,\gamma = x,y,z$) is a third-order tensor ($3\times3\times3$) and represents the spin current $J^\gamma_{s,\alpha}$ generated by an electric field **E** via $J^\gamma_{s,\alpha} = \sigma^\gamma_{\alpha\beta}E_\beta$, where $J^\gamma_{s,\alpha}$ is a spin current flowing along the α-direction with the spin-polarization along the γ-direction.

We know that AHE vanishes while SHE remains if the time-reversal symmetry (operator T) exists in the system. In Eq. 2, T reverses the velocities $\hat{v}_{\alpha,\beta}$ and brings an additional "$-$" sign by the complex conjugate. Thus, $\sigma_{\alpha\beta} = 0$ owing to $\Omega_{n,\alpha\beta}(\vec{k}) = -\Omega_{n,\alpha\beta}(-\vec{k})$. In contrast, In Eq. 3, T generates one more "$-$" sign by reversing the spin in J^γ_α. Then, $\sigma^\gamma_{\alpha\beta}$ can be nonzero since $\Omega^\gamma_{n,\alpha\beta}(\vec{k})$ is even in k-space. When SOC is absent or negligible, a magnetic system usually exhibits the spin rotation symmetry (operator S), which rotates only spins (or magnetic moments) simultaneously but not the lattice. Although T is broken here, some systems may still preserve a combined symmetry by T and a spin-rotation of 180° degree, noted as TS. For example, a coplanar magnetic system shows a TS symmetry, in which S rotates all spins by 180° around the axis perpendicular to the plane. Since S does not act on $\hat{v}_{\alpha,\beta}$, TS causes vanishing $\sigma_{\alpha\beta}$ just as T alone. In a general noncoplanar magnetic lattice, the TS symmetry is naturally broken, because one cannot find a common axis about which all spins can be rotated 180° at the same time, and thus the AHE can exist without SOC.

The situation is different for the SHE since J^γ_α in Eq. 3 contains an additional spin operator. As a consequence, (assuming that S is a rotation around the z axis) TS forces $\Omega^{x/y}_{n,\alpha\beta}(\vec{k})$ to be odd where spin $\hat{s}_x$ or $\hat{s}_y$ is reversed by TS, but $\Omega^z_{n,\alpha\beta}(\vec{k})$ to be even where $\hat{s}_z$ is unchanged by TS. Then, one can obtain zero $\sigma^{x/y}_{\alpha\beta}$ but nonzero $\sigma^z_{\alpha\beta}$. In a collinear magnetic lattice there exists more than one spin rotation S such that TS is a symmetry of the system

and thus all of the $\sigma^{\gamma}_{\alpha\beta}$ components have to vanish. Therefore, we can argue that SHE can exist without SOC in general noncollinear magnetic lattices, regardless of FM, AFM, or the scalar spin chirality (coplanar or noncoplanar). In contrast, the AHC is zero for a coplanar magnetic lattice (zero scalar spin chirality), since TS acts as T alone in Eq. 2.

When SOC is included, SHE is allowed by symmetry in any crystal[29], while the AHE on the other hand can be present in magnetic systems that are not symmetric under time reversal combined with a translation or inversion (for example, a conventional collinear AFM). We summarize the necessary conditions for the existence of AHE and SHE in systems with and without SOC in Fig. 1.

To demonstrate that the SHE can indeed be nonzero without SOC, we consider the s–d Hamiltonian (1) projected on a kagome lattice with the so-called $q = 0$ magnetic order, shown in Fig. 2(a). Such a coplanar AFM order is well studied in theory [14, 30] and appears in many realistic materials even at room temperature, for example Mn_3X (X = Ir, Ga, Ge, and Sn) [24, 25, 31–34] as we discuss in the following. For comparison, the SOC effect is also considered by adding to H in Eq. 1,

$$H_{\rm so} = it_2 \sum_{<ij>\alpha\beta} v_{ij}(\boldsymbol{\sigma}\cdot\boldsymbol{n}_{ij})_{\alpha\beta} c^{\dagger}_{i\alpha} c_{j\beta}, \tag{4}$$

where v_{ij} and n_{ij} are defined as in Ref. 30 and t_2 is the SOC strength.

We first analyze the symmetry of the SHC tensor for the $q = 0$ magnetic order. Note that we use the Cartesian coordinate systems defined in Fig. 2. As discussed above, the existence of the TS symmetry leaves only $\sigma^{z}_{\alpha\beta}$ terms in the absence of SOC. Further, the combined symmetry TM_x, in which M_x is the mirror reflection along x and flips $\hat{s}_z$ and $\hat{v}_x$ in Eq. 3, leads to $\sigma^{z}_{xx} = \sigma^{z}_{yy} = 0$. We further obtain only two nonzero SHC tensor element $\sigma^{z}_{xy} = -\sigma^{z}_{yx}$ by considering the three-fold rotation around z. The magnetic order shown in Fig. 2(b) will also be relevant for the discussion in the following. This magnetic configuration differs from the $q = 0$ case only by a two-fold spin rotation around the y-axis and thus, without SOC its symmetry is exactly the same as that of the $q = 0$ case.

Setting the Hund coupling constant $J = 1.7t$ and SOC strength $t_2 = 0$, we calculate the spin Berry curvature via Eq. 3. As expected, we find nonzero SHC σ^{z}_{xy} fully in agreement with the symmetry considerations. Figures 3a and 3b show the band structures with $t_2 = 0$ and $t_2 = 0.2t$, respectively. One can see that SOC modifies slightly the band structure by gaping some band crossing points such as the BZ corners (K). Without SOC, we already

observe nonzero σ^z_{xy}, while adding SOC reduces σ^z_{xy} slightly at the Fermi energy that is set between the first and second bands at about –2.7 eV. We plot corresponding spin Berry curvature Ω^z_{xy} in the hexagonal BZ In Figs. 3d and 3e. Large Ω^z_{xy} appears in the BZ without SOC, leading to net σ^z_{xy}. The SOC simply brings an extra contribution to σ^z_{xy} at the band anti-crossing region around the K point.

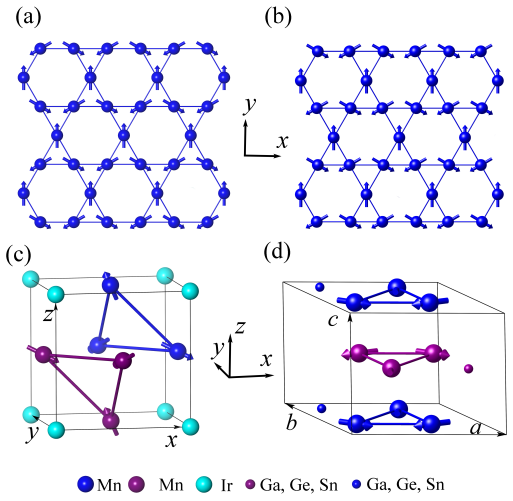

FIG. 2. Noncollinear order in kagome lattice and the magnetic structure of Mn_3Ir and Mn_3X (X = Ga, Ge, and Sn). (a) The $q = 0$ order in the kagome lattice, with magnetic moments located as 2D Mn plane in Mn_3Ir, (b) Two-fold spin rotation around y-axis of configuration (a), corresponding to Mn planes in Mn_3X (X = Ga, Ge, Sn), (c) The face-centered cubic crystal structure of Mn_3Ir, (d) The hexagonal crystal structure of Mn_3X (X = Ga, Ge, and Sn).

Realistic materials – After proving the principle, we now identify materials that show strong SHE with negligible contribution from SOC. We naturally consider Mn_3X (X=Ga, Ge, Sn, and Ir) compounds, since they exhibit non-collinear AFM order at room temperature (the AFM Néel temperature is over 365 K). Our recent *ab initio* calculations showed a sizable intrinsic SHE by including SOC [34]. Here, we further point out that SHE still presents without SOC and SOC actually plays a negligible effect for SHE in these materials.

The primitive unit cell of Mn_3Ga, Mn_3Ge and Mn_3Sn (space group $P6_3/mmc$, No. 194) includes two Mn_3X planes that are stacked along the c-axis according to a "–AB–AB–" sequence. Inside each plane, Mn atoms form a kagome-type lattice with Ga, Ge, or Sn lying at the center of the hexagon formed by Mn. Both the *ab initio* calculation [31] and

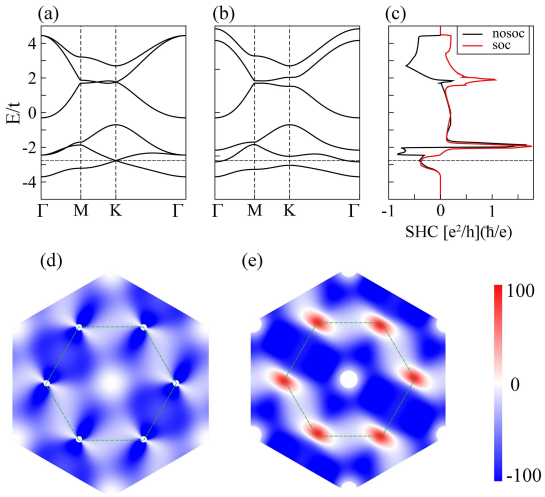

FIG. 3. Electronic band structures $q = 0$ order in kagome lattice, (a) without SOC, (b) with SOC. (c) Energy-dependent SHC σ^z_{xy}. (d) Spin Berry curvature Ω^z_{xy} distribution of first BZ at Fermi energy -2.7 eV (horizontal line) without SOC and (e) with SOC.

neutron diffraction measurements [35–37] show that the Mn magnetic moments exhibit noncollinear AFM order, where the neighboring moments are aligned at an angle of 120°, as in Fig. 2(b). Large AHE in room temperature has recently been reported in Mn_3Ge and Mn_3Sn [24, 25]. These materials also exhibit other exotic phenomena including the Weyl semimetal phase [38], magneto-optical Kerr effect [39], anomalous Nernst effect [40], and topological defects [41]. Distinct from hexagonal Mn_3X compounds, the Mn_3Ir (space group $Pm\bar{3}m$, No. 221) crystallizes in a face-centered cubic structure with Mn atoms in the [111] planes forming a kagome lattice with the $q = 0$ magnetic order.

The symmetry of the SHE without SOC in these materials can be understood using a similar approach as we used for the 2D kagome lattice. The hexagonal Ga, Ge, and Sn materials can be viewed as stacking versions of the kagome lattice and thus we find that the symmetry of SHE is the same as the 2D kagome lattice, i.e. only $\sigma^z_{xy} = -\sigma^z_{yx}$ is nonzero. However, we find that SHE must vanish in Mn_3Ir without SOC, which is imposed by the higher symmetry of the cubic magnetic lattice. For completeness, we list the tensor matrices without and with SOC for all these compounds in the appendix.

Since the SHC tensor shape imposed by the symmetry has been systematically investigated for these materials in Ref. [34], we only discuss one of the largest SHC tensor elements

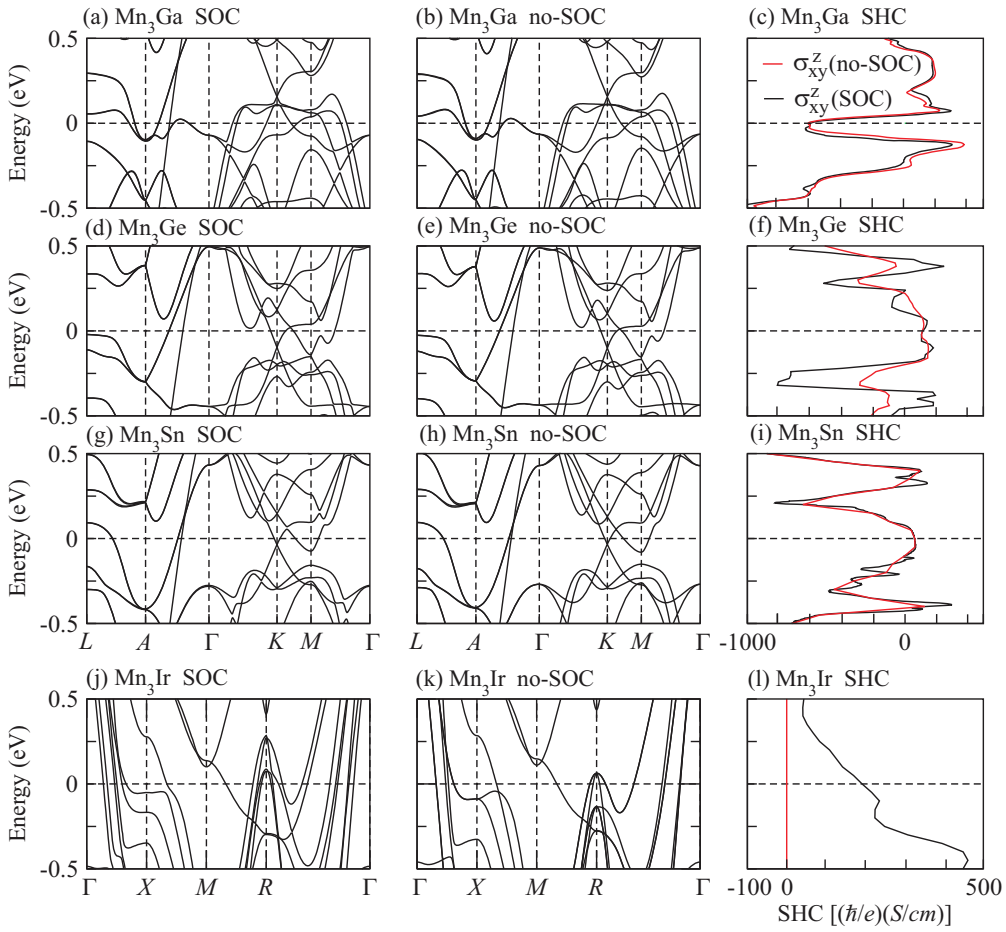

FIG. 4. Electronic band structure for (a) Mn_3Ga with SOC, (b) Mn_3Ga without SOC, (d) Mn_3Ge with SOC, (e) Mn_3Ge without SOC, (g) Mn_3Sn with SOC, (h) Mn_3Sn without SOC, (j) Mn_3Ir with SOC, (k) Mn_3Ir without SOC. Energy-dependent SHC tensor elements of σ^z_{xy} with and without SOC for (c) Mn_3Ga, (f) Mn_3Ge, (i) Mn_3Sn, and (l) Mn_3Ir. The Fermi energy is indicated by the dashed horizontal line.

σ^z_{xy} based on the *ab initio* calculations [42] of the SHC. For comparison, we show the band structure and SHC without and together with SOC in Fig. 4. In the absence of SOC, Ga, Ge, and Sn compounds indeed exhibit nonzero SHC $\sigma^z_{xy} = -613, 115, 90\ (\hbar/e)(\Omega \cdot cm)^{-1}$, respectively, at the Fermi energy. One can see that SOC induces very few changes in the band structure and thereafter modifies the SHC weakly, especially at the Fermi energy for Ga, Ge, and Sn compounds. It is intuitive to observe comparable σ^z_{xy} values for Ge and Sn compounds, despite the fact that Sn exhibits much larger SOC than Ge. These facts further verifies that the noncollinear magnetic structure, rather than SOC, is dominant for the SHE.

The Ga compound shows an opposite sign in SHC compared to the Ge/Sn compound, since Ga has one valence electron fewer than Ge/Sn and the Fermi energy is lower in Mn_3Ga than in Mn_3Ge/Mn_3Sn.

Summary – We proposed that the SHE can be realized by a chiral magnetic structure without involving the SOC. The noncollinearity of the chiral magnetic lattice can break the spin rotation symmetry and consequently allow the existence of SHE. By *ab initio* calculations, we further predicted that such an SHE without SOC can be observed in noncollinear AFM compounds Mn_3X (X = Ga, Ge, and Sn). Although only the intrinsic SHE is considered here, we expect that an extrinsic SHE can also appear commonly in the chiral magnetic lattice without SOC because of similar symmetry considerations. By enabling a new understanding of the SHE, our work paves the way to search for SHE materials among chiral magnetic systems, which are not limited to the heavy element materials. In addition, the close relation between SHE and the magnetic order suggests that SHE may be used as a probe for different magnetic structures.

We thank Prof. Claudia Felser at MPI-CPfS and Prof. Carsten Timm at TU-Dresden for helpful discussions. Y.Z. and J.v.d.B. acknowledge the German Research Foundation (DFG) SFB 1143. B.Y. thanks the support of the Ruth and Herman Albert Scholars Program for New Scientists in Weizmann Institute of Science, Israel.

* binghai.yan@weizmann.ac.il

[1] J. Sinova, S. O. Valenzuela, J. Wunderlich, C. Back, and T. Jungwirth, Reviews of Modern Physics **87** (2015).

[2] S. A. Wolf, D. D. Awschalom, R. A. Buhrman, J. M. Daughton, S. von Molnár, M. L. Roukes, A. Y. Chtchelkanova, and D. M. Treger, Science **294**, 1488 (2001).

[3] S. Maekawa, S. O. Valenzuela, E. Saitoh, and T. Kimura, *Spin Current*, Vol. 17 (Oxford University Press, 2012).

[4] A. Hoffmann, IEEE Trans. Magn. **49**, 5172 (2013).

[5] M. Gradhand, D. Fedorov, F. Pientka, P. Zahn, I. Mertig, and B. L. Györffy, Journal of Physics: Condensed Matter **24**, 213202 (2012).

[6] I. M. Miron, K. Garello, G. Gaudin, P.-J. Zermatten, M. V. Costache, S. Auffret, S. Bandiera,

B. Rodmacq, A. Schuhl, and P. Gambardella, Nature **476**, 189 (2011).

[7] L. Liu, C.-F. Pai, Y. Li, H. W. Tseng, D. C. Ralph, and R. A. Buhrman, Science **336**, 555 (2012).

[8] S. Parkin and S.-H. Yang, Nature Nanotech **10**, 195 (2015).

[9] S.-H. Yang, K.-S. Ryu, and S. Parkin, Nature Nanotech **10**, 221 (2015).

[10] N. Nagaosa, J. Sinova, S. Onoda, A. H. MacDonald, and N. P. Ong, Reviews of Modern Physics **82**, 1539 (2010).

[11] S. Murakami, N. Nagaosa, and S.-C. Zhang, Science **301**, 1348 (2003).

[12] J. Sinova, D. Culcer, Q. Niu, N. A. Sinitsyn, T. Jungwirth, and A. H. MacDonald, Phys. Rev. Lett. **92**, 126603 (2004).

[13] D. Xiao, M.-C. Chang, and Q. Niu, Rev. Mod. Phys. **82**, 1959 (2010).

[14] K. Ohgushi, S. Murakami, and N. Nagaosa, Physical Review B **62**, R6065 (2000).

[15] Y. Taguchi, Y. Oohara, H. Yoshizawa, N. Nagaosa, and Y. Tokura, Science **291**, 2573 (2001).

[16] P. Bruno, V. K. Dugaev, and M. Taillefumier, Phys. Rev. Lett. **93**, 096806 (2004).

[17] A. Neubauer, C. Pfleiderer, B. Binz, A. Rosch, R. Ritz, P. G. Niklowitz, and P. Böni, Phys. Rev. Lett. **102**, 186602 (2009).

[18] N. Kanazawa, Y. Onose, T. Arima, D. Okuyama, K. Ohoyama, S. Wakimoto, K. Kakurai, S. Ishiwata, and Y. Tokura, Phys. Rev. Lett. **106**, 156603 (2011).

[19] G. Yin, Y. Liu, Y. Barlas, J. Zang, and R. K. Lake, Phys. Rev. B **92**, 024411 (2015).

[20] P. M. Buhl, F. Freimuth, S. Blügel, and Y. Mokrousov, arXiv:1701.03030 (2017).

[21] Y. Tserkovnyak, A. Brataas, and G. E. W. Bauer, Phys. Rev. Lett. **88**, 117601 (2002).

[22] G. Guo, S. Murakami, T.-W. Chen, and N. Nagaosa, Physical review letters **100**, 096401 (2008).

[23] T. Tanaka, H. Kontani, M. Naito, T. Naito, D. S. Hirashima, K. Yamada, and J. Inoue, Physical Review B **77**, 165117 (2008).

[24] A. K. Nayak, J. E. Fischer, Y. Sun, B. Yan, J. Karel, A. C. Komarek, C. Shekhar, N. Kumar, W. Schnelle, J. Kuebler, C. Felser, and S. S. P. Parkin, Science Advances **2**, 150187 (2016).

[25] S. Nakatsuji, N. Kiyohara, and T. Higo, Nature **527**, 212 (2015).

[26] C. Zener, Phys. Rev. **82**, 403 (1951).

[27] P. W. Anderson and H. Hasegawa, Phys. Rev. **100**, 675 (1955).

[28] P. G. de Gennes, Phys. Rev. **118**, 141 (1960).

[29] M. Seemann, D. Koedderitzsch, S. Wimmer, and H. Ebert, Physical Review B **92**, 155138 (2015).

[30] H. Chen, Q. Niu, and A. MacDonald, Phys. Rev. Lett. **112**, 017205 (2014).

[31] D. Zhang, B. Yan, S.-C. Wu, J. Kübler, G. Kreiner, S. S. Parkin, and C. Felser, Journal of Physics: Condensed Matter **25**, 206006 (2013).

[32] J. Kübler and C. Felser, EPL **108**, 67001 (2014).

[33] W. Zhang, W. Han, S. H. Yang, Y. Sun, Y. Zhang, B. Yan, and S. Parkin, Science Advances **2**, e1600759 (2016).

[34] Y. Zhang, Y. Sun, H. Yang, J. Železný, S. P. P. Parkin, C. Felser, and B. Yan, Phys. Rev. B **95**, 075128 (2017).

[35] E. Krén and G. Kádár, Solid State Communications **8**, 1653 (1970).

[36] G. Kádár and E. Krén, International Journal of Magnetism **1**, 43 (1971).

[37] T. Ohoyama, K. Yasukchi, and K. Kanematsu, Phys. Soc. Japan **16**, 325 (1961).

[38] H. Yang, Y. Sun, Y. Zhang, W.-J. Shi, S. S. P. Parkin, and B. Yan, arXiv:1608.03404 (2016).

[39] W. Feng, G.-Y. Guo, J. Zhou, Y. Yao, and Q. Niu, Phys. Rev. B **92**, 144426 (2015).

[40] X. Li, L. Xu, L. Ding, J. Wang, M. Shen, X. Lu, Z. Zhu, and K. Behnia, arXiv:1612.06128 (2016).

[41] J. Liu and L. Balents, arXiv:1703.08910 (2017).

[42] G. Kresse and J. Furthmüller, Phys. Rev. B **54**, 11169 (1996).

APPENDIX

TABLE I. Shape of the AHC and SHC tensors obtained from symmetry analysis and numerical calculations for Mn_3X (X=Ga, Ge, and Sn). The calculated SHC tensor elements are set to zero when they are less than 5 $(\hbar/e)(\Omega \cdot cm)^{-1}$. The coordinates used here are x along [100], y along [120], and z along [001], as presented in Fig. 1(a, b). The SHC are given in units of $(\hbar/e)(\Omega \cdot cm)^{-1}$.

	AHC	SHC		
	σ	$\underline{\sigma}^x$	$\underline{\sigma}^y$	$\underline{\sigma}^z$
tensor shape with soc	$\begin{pmatrix} 0 & 0 & -\sigma_{zx} \\ 0 & 0 & 0 \\ \sigma_{zx} & 0 & 0 \end{pmatrix}$	$\begin{pmatrix} 0 & 0 & 0 \\ 0 & 0 & \sigma^x_{yz} \\ 0 & \sigma^x_{zy} & 0 \end{pmatrix}$	$\begin{pmatrix} 0 & 0 & \sigma^y_{xz} \\ 0 & 0 & 0 \\ \sigma^y_{zx} & 0 & 0 \end{pmatrix}$	$\begin{pmatrix} 0 & \sigma^z_{xy} & 0 \\ \sigma^z_{yx} & 0 & 0 \\ 0 & 0 & 0 \end{pmatrix}$
Mn_3Ga	$\begin{pmatrix} 0 & 0 & -81 \\ 0 & 0 & 0 \\ 81 & 0 & 0 \end{pmatrix}$	$\begin{pmatrix} 0 & 0 & 0 \\ 0 & 0 & -15 \\ 0 & 12 & 0 \end{pmatrix}$	$\begin{pmatrix} 0 & 0 & 15 \\ 0 & 0 & 0 \\ -7 & 0 & 0 \end{pmatrix}$	$\begin{pmatrix} 0 & -597 & 0 \\ 625 & 0 & 0 \\ 0 & 0 & 0 \end{pmatrix}$
Mn_3Ge	$\begin{pmatrix} 0 & 0 & 330 \\ 0 & 0 & 0 \\ -330 & 0 & 0 \end{pmatrix}$	$\begin{pmatrix} 0 & 0 & 0 \\ 0 & 0 & -21 \\ 0 & 18 & 0 \end{pmatrix}$	$\begin{pmatrix} 0 & 0 & 21 \\ 0 & 0 & 0 \\ -18 & 0 & 0 \end{pmatrix}$	$\begin{pmatrix} 0 & 112 & 0 \\ -115 & 0 & 0 \\ 0 & 0 & 0 \end{pmatrix}$
Mn_3Sn	$\begin{pmatrix} 0 & 0 & 133 \\ 0 & 0 & 0 \\ -133 & 0 & 0 \end{pmatrix}$	$\begin{pmatrix} 0 & 0 & 0 \\ 0 & 0 & -36 \\ 0 & 96 & 0 \end{pmatrix}$	$\begin{pmatrix} 0 & 0 & 36 \\ 0 & 0 & 0 \\ -96 & 0 & 0 \end{pmatrix}$	$\begin{pmatrix} 0 & 64 & 0 \\ -68 & 0 & 0 \\ 0 & 0 & 0 \end{pmatrix}$
tensor shape without soc	$\begin{pmatrix} 0 & 0 & 0 \\ 0 & 0 & 0 \\ 0 & 0 & 0 \end{pmatrix}$	$\begin{pmatrix} 0 & 0 & 0 \\ 0 & 0 & 0 \\ 0 & 0 & 0 \end{pmatrix}$	$\begin{pmatrix} 0 & 0 & 0 \\ 0 & 0 & 0 \\ 0 & 0 & 0 \end{pmatrix}$	$\begin{pmatrix} 0 & \sigma^z_{xy} & 0 \\ -\sigma^z_{xy} & 0 & 0 \\ 0 & 0 & 0 \end{pmatrix}$
Mn_3Ga	$\begin{pmatrix} 0 & 0 & 0 \\ 0 & 0 & 0 \\ 0 & 0 & 0 \end{pmatrix}$	$\begin{pmatrix} 0 & 0 & 0 \\ 0 & 0 & 0 \\ 0 & 0 & 0 \end{pmatrix}$	$\begin{pmatrix} 0 & 0 & 0 \\ 0 & 0 & 0 \\ 0 & 0 & 0 \end{pmatrix}$	$\begin{pmatrix} 0 & -613 & 0 \\ 631 & 0 & 0 \\ 0 & 0 & 0 \end{pmatrix}$
Mn_3Ge	$\begin{pmatrix} 0 & 0 & 0 \\ 0 & 0 & 0 \\ 0 & 0 & 0 \end{pmatrix}$	$\begin{pmatrix} 0 & 0 & 0 \\ 0 & 0 & 0 \\ 0 & 0 & 0 \end{pmatrix}$	$\begin{pmatrix} 0 & 0 & 0 \\ 0 & 0 & 0 \\ 0 & 0 & 0 \end{pmatrix}$	$\begin{pmatrix} 0 & 115 & 0 \\ -115 & 0 & 0 \\ 0 & 0 & 0 \end{pmatrix}$
Mn_3Sn	$\begin{pmatrix} 0 & 0 & 0 \\ 0 & 0 & 0 \\ 0 & 0 & 0 \end{pmatrix}$	$\begin{pmatrix} 0 & 0 & 0 \\ 0 & 0 & 0 \\ 0 & 0 & 0 \end{pmatrix}$	$\begin{pmatrix} 0 & 0 & 0 \\ 0 & 0 & 0 \\ 0 & 0 & 0 \end{pmatrix}$	$\begin{pmatrix} 0 & 90 & 0 \\ -90 & 0 & 0 \\ 0 & 0 & 0 \end{pmatrix}$

TABLE II. Intrinsic SHC tensors obtained from symmetry analysis and numerical calculations for Mn_3Ir. The calculated SHC tensor elements are set to zero when they are less than 2 $(\hbar/e)(\Omega{\cdot}cm)^{-1}$. The coordinate axes correspond to z oriented in the [111] direction, x along $[1\bar{1}0]$ and y along $[11\bar{2}]$. The SHC are in units of $(\hbar/e)(\Omega \cdot cm)^{-1}$.

	AHC	SHC		
	σ	$\underline{\sigma}^x$	$\underline{\sigma}^y$	$\underline{\sigma}^z$
tensor shape with soc	$\begin{pmatrix} 0 & \sigma_{xy} & 0 \\ -\sigma_{xy} & 0 & 0 \\ 0 & 0 & 0 \end{pmatrix}$	$\begin{pmatrix} \sigma^x_{xx} & 0 & 0 \\ 0 & -\sigma^x_{xx} & -\sigma^x_{yz} \\ 0 & \sigma^x_{zy} & 0 \end{pmatrix}$	$\begin{pmatrix} 0 & -\sigma^x_{xx} & -\sigma^x_{yz} \\ -\sigma^x_{xx} & 0 & 0 \\ -\sigma^x_{zy} & 0 & 0 \end{pmatrix}$	$\begin{pmatrix} 0 & \sigma^z_{xy} & 0 \\ -\sigma^z_{xy} & 0 & 0 \\ 0 & 0 & 0 \end{pmatrix}$
Mn_3Ir	$\begin{pmatrix} 0 & -312 & 0 \\ 312 & 0 & 0 \\ 0 & 0 & 0 \end{pmatrix}$	$\begin{pmatrix} -210 & 0 & 0 \\ 0 & 210 & 299 \\ 0 & -7 & 0 \end{pmatrix}$	$\begin{pmatrix} 0 & 210 & -299 \\ 210 & 0 & 0 \\ 7 & 0 & 0 \end{pmatrix}$	$\begin{pmatrix} 0 & 163 & 0 \\ -163 & 0 & 0 \\ 0 & 0 & 0 \end{pmatrix}$
tensor shape without soc	$\begin{pmatrix} 0 & 0 & 0 \\ 0 & 0 & 0 \\ 0 & 0 & 0 \end{pmatrix}$	$\begin{pmatrix} 0 & 0 & 0 \\ 0 & 0 & 0 \\ 0 & 0 & 0 \end{pmatrix}$	$\begin{pmatrix} 0 & 0 & 0 \\ 0 & 0 & 0 \\ 0 & 0 & 0 \end{pmatrix}$	$\begin{pmatrix} 0 & 0 & 0 \\ 0 & 0 & 0 \\ 0 & 0 & 0 \end{pmatrix}$
Mn_3Ir	$\begin{pmatrix} 0 & 0 & 0 \\ 0 & 0 & 0 \\ 0 & 0 & 0 \end{pmatrix}$	$\begin{pmatrix} 0 & 0 & 0 \\ 0 & 0 & 0 \\ 0 & 0 & 0 \end{pmatrix}$	$\begin{pmatrix} 0 & 0 & 0 \\ 0 & 0 & 0 \\ 0 & 0 & 0 \end{pmatrix}$	$\begin{pmatrix} 0 & 0 & 0 \\ 0 & 0 & 0 \\ 0 & 0 & 0 \end{pmatrix}$